Development of an AFM-Based System for In-Process Measurement of Micro-Defects on Machined Surfaces*

Hyun-Kyu KWEON**, Wei GAO***
Tsunemoto KURIYAGAWA*** and Satoshi KIYONO***

This paper examines a new in-process measurement system for the measurement of micro-defects on the surfaces of brittle materials by using the AFM (Atomic Force Microscopy). A new AFM scanning stage that can also perform nano-scale bending of the sample was developed by adding a bending unit to a commercially available AFM scanner. The bending unit consists of a PZT actuator and sample holder, and can perform static and cyclic three-point bending. The true bending displacement of the bending unit is approximately 1.8 μm when 80 volts are applied to the PZT actuator. The frequency response of the bending unit and the stress on the sample were also analyzed, both theoretically and experimentally. Potential surface defects of the sample were successfully detected by this measurement system. It was confirmed that the number of micro-defects on a scratched surface increases when the surface is subjected to a cyclic bending load.

Key Words: Measurement, Atomic Force Microscopy, Micro-Defects, Bending, In-Process

1. Introduction

The mechanical surface properties of ultra-fine finished brittle materials, such as silicon wafers, are greatly affected by surface defects. To clarify the mechanism through which defects occur, it is essential to observe and measure the defects in real time while external stress is being applied to the surface[1]. Moreover, in-process measurement can be said to be essential to observe potential defects. In most cases, however, the surface defects of brittle materials are quite small[2]. Some of them are on the nanometric scale. It is extremely difficult to identify such micro-defects, especially under in-process conditions.

Recently, several in-process measurement methods using optical microscopy[1],[3] or scanning electron microscopy (SEM)[4],[5] have been proposed to observe surface defects. Both the optical microscope and SEM have long depths of field, fast imaging speeds and high vertical resolution. However, the optical microscope has low lateral resolution. Two disadvantages of SEM are that the sample must be placed in a vacuum, and the surface must be conductive. In addition, the height and depth of the defect cannot be accurately measured because the SEM image is a two-dimensional projection of a three dimensional sample.

Atomic force microscopy (AFM) is becoming one of the most powerful tools to study the nanometric structures of surfaces[6]. AFM has both lateral and vertical atomic resolution, and is capable of providing high speed quantitative three-dimensional information about the sample. It can also image nonconducting materials without placing the sample in a vacuum. Considering that most brittle materials are nonconducting or semiconducting, and that most processes are not performed in a vacuum, AFM is expected to provide the most feasible approach to the problem of in-process measurement of the growth of micro-defects on the surface of brittle materials.

* Received 21st November, 1997
** Graduate School, Tohoku University, Sendai 980-8579, Japan
*** Department of Mechatronics, Faculty of Engineering, Tohoku University, Japan. E-mail: kiyono@cc.mech.tohoku.ac.jp

In the present study, a new system has been developed and investigated that makes in-process nano-measurement of surface defects possible, including potential defects, by utilizing AFM. An unique bending unit that can perform three-point bending was added to a commercially available AFM scanning stage. The bending load is controlled by a PZT actuator. The sample can be imaged by AFM while being bent by the bending unit. The basic characteristics of the new system were investigated, and the growth of micro-defects was measured in real time during bending and repeat-bending processes.

2. In-Process Measurement System

2.1 Configuration of the system

Figure 1 shows the configuration of the newly developed in-process measurement system. A bending unit capable of three-point bending was added to a commercially available AFM scanning stage. Figure 2 shows a schematic of the bending unit. The bending unit consists of a PZT actuator, the sample and sample holder. A single-crystal silicon sample was used. The two ends of the sample are fixed by the sample holder, and the center of the sample is driven by the PZT actuator. The PZT actuator is used as a load generator to bend the sample. The sample can be measured by AFM during the bending process.

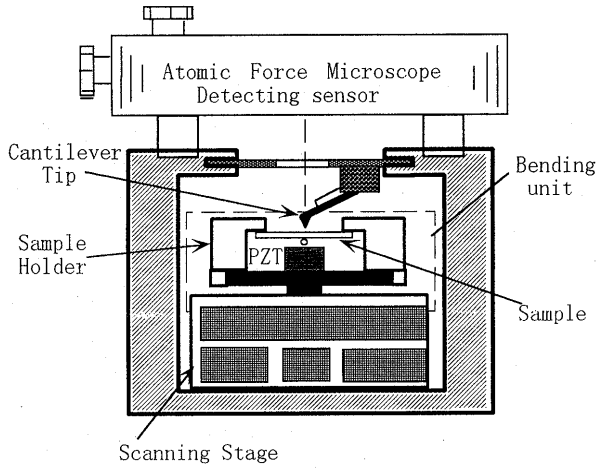

Fig. 1 In-process measurement system

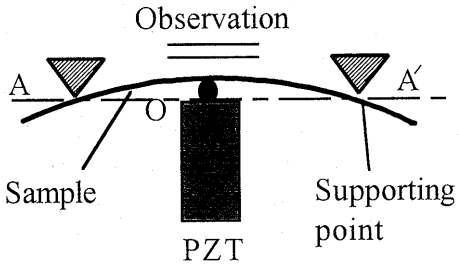

Fig. 2 Bending method

2.2 Performance of the bending unit

2.2.1 Bending displacement The bending displacement of the center point O of the sample does not match the stretching displacement of the PZT actuator because of the displacement at fulcrum points A and A′. To identify the true bending displacement of the bending unit, capacitance-type displacement probes (Microsense) are employed. As shown in Fig. 3, the displacements are measured at points A and O. As a result, the true bending displacement can be evaluated by the difference between the displacements at the two points. As shown in Fig. 4, the true bending displacement is approximately 1.8 μm when 80 volts are applied to the PZT actuator. It is also shown that the displacement at point A′ does not differ from that at point A.

2.2.2 Frequency response of the bending unit In the case of repeat-bending, it is necessary to determine the frequency range of external force in which irregular vibration of the bending unit does not occur. For this purpose, the frequency response of the bending unit was investigated experimentally. As shown in Fig. 5, the vibration frequency limit f_t of external force is approximately 20 kHz.

2.2.3 Stress analysis of the sample during bending During upward bending, the stress in a vertical cross section of the sample is a linear function of the depth, ranging from maximum tension $+\sigma_{max}$ in the upper surface to maximum compression $-\sigma_{max}$ in the bottom surface[7]. The bending equation can be expressed as follows:

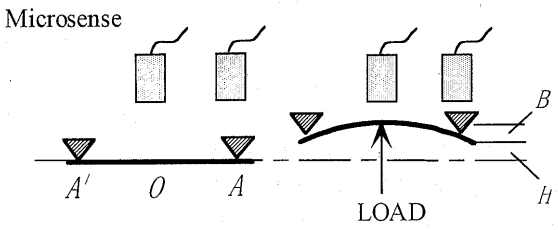

Fig. 3 True bending displacement (B: True bending displacement, H: supporting displacement)

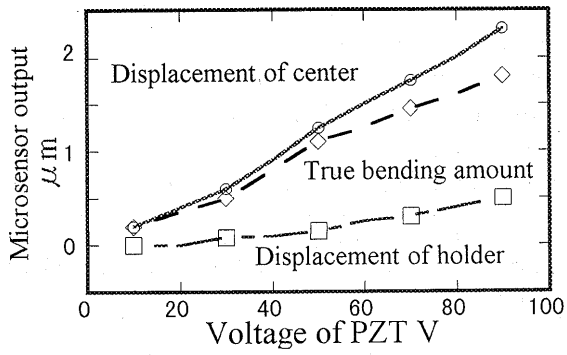

Fig. 4 Measured bending displacement

$$\frac{EId^2y}{d^2x}=M, \quad (1)$$

where E is the modulus of elasticity and I is the second of moment of area. From Eq.(1), the relationship between the maximum moment M_{max} and beam deflection δ at the center position of the beam during rotation can be obtained as follows:

$$M_{max}=\frac{12EI\delta}{L^2}, \quad (2)$$

where L is the beam length. The relationship between the maximum stress σ_{max} and the maximum moment M_{max} can be determined as:

$$\sigma_{max}=\frac{Et}{2R}=\frac{M_{max}t}{2I}, \quad (3)$$

where t is the beam thickness and R is the bending radius. From Eqs.(2) and (3), the theoretical value of maximum stress σ_{max} can be obtained as follows:

$$\sigma_{max}=\frac{6Et\delta}{L^2}. \quad (4)$$

In addition, Eq.(3) can also be used to determine the external force P as follows

$$P=\frac{2\sigma_{max}bt}{3L}, \quad (5)$$

where b is the beam width.

From Eqs.(1) to (5), the stress and the external bending force are calculated to be 780 kPa and 42 mN, respectively, under $E=130$ GPa, $t=200$ μm, $b=20$ mm and $\delta=0.5$ μm. In addition the external force P was evaluated by Eq.(5), and measured by a digital force-gauge (DFG-0.2K, SIMPO). Figure 6 shows the results. Because a simple mathematical model was adopted for simplicity, the two results in Fig. 6 do not agree well with each other. It is possible to carry out a more complete stress evaluation by employing the finite-element technique. However, the geometry of our test specimens is affected by some uncertainties, for example, those concerning nonrectangular beam cross sections. Therefore, it was felt that a more detailed approach would be overly complex.

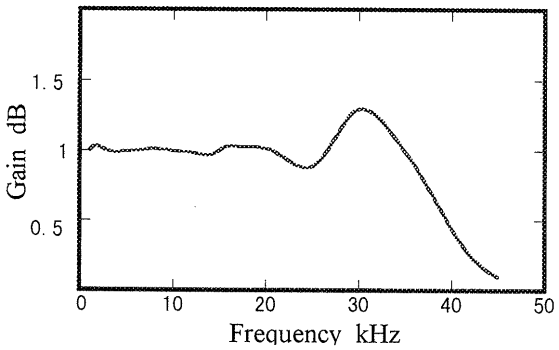

Fig. 5 Frequency response of the bending unit

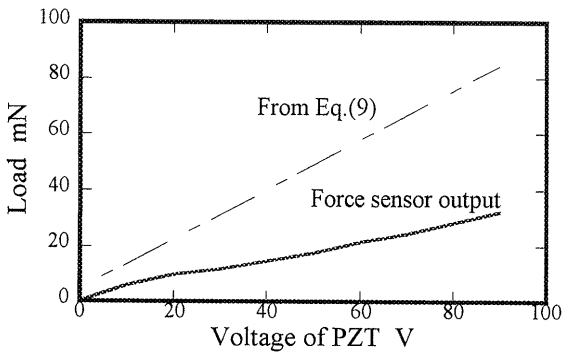

Fig. 6 Comparision of forcesensor and formule (9)

3. Experiment Results

Two kinds of experiments were performed to detect potential surface defects during the bending process. One was a static bending test, and the other was a cyclic-bending test.

3.1 Measurement in bending process

In the first experiment, potential micro-defects on the surface were observed. A sample, which had been scratched by using a micro-machining test machine[8], was placed on the AFM bending unit. The sample surface was measured using AFM before the bending test.

Next, the sample was bent, and was measured again by AFM while the bending state was maintained. Figs. 7(a) and 7(b) show the AFM images measured before bending and during bending. As shown in Fig. 7(b), the potential micro-defect was detected clearly in the second measurement. The measurement was performed again when the bending was released. Figure 7(c) shows the measured result. The defect, which was observed during bending, can not be observed. This result confirms that potential surface defects can be detected by the new measurement system.

3.2 Measurement during the cyclic-bending process

In the second experiment, the effect of cyclic-bending was investigated. Two kinds of samples were used. Sample 1 is the same as that used in the first experiment. Sample 2 has an indentation mark made using a dynamic ultra-microhardness tester.

A function generator was used as the bending stage controller to apply a cyclic bending load to the sample. Table 1 shows the conditions of the cyclic-bending test. Fig. 8 shows the results of sample 1 measured after cyclic-bending for 90 minutes. Figure 9 plots of the change in the depth of defects versus repeat time. It shown that the width of the micro-defects on the machined surface is increased by cyclic-bending in proportion to the repeat time. As can be seen in Figs. 7 and 8, under the experimental conditions described above, elastic deformation occurred in the static bending process, and plastic deformation occurred in the cyclic-bending process.

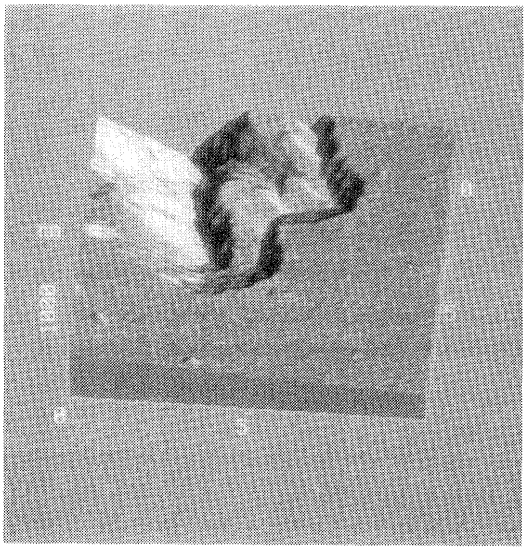

Fig. 7(a) Measured results of bending

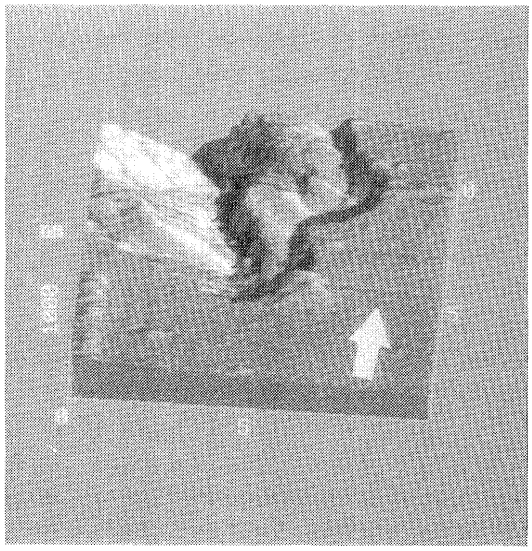

Fig. 7(b) Measured results of bending

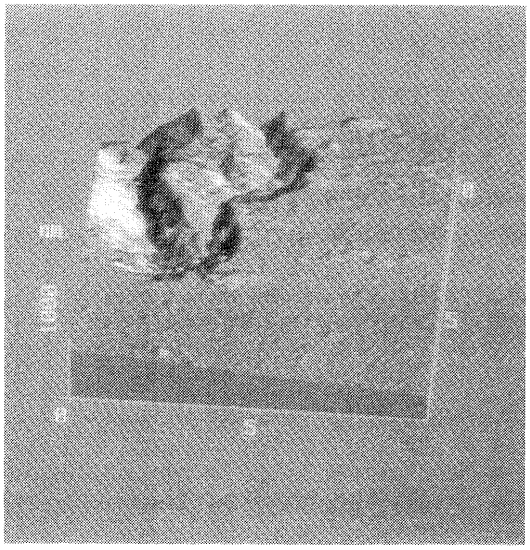

Fig. 7(c) Measured results of bending

Table 1 Experiment condition

Experiment condition	Deflection of sample	Frequency	Repeating time
Amount	500nm	10kHz	30, 60, 90, and 120 minutes

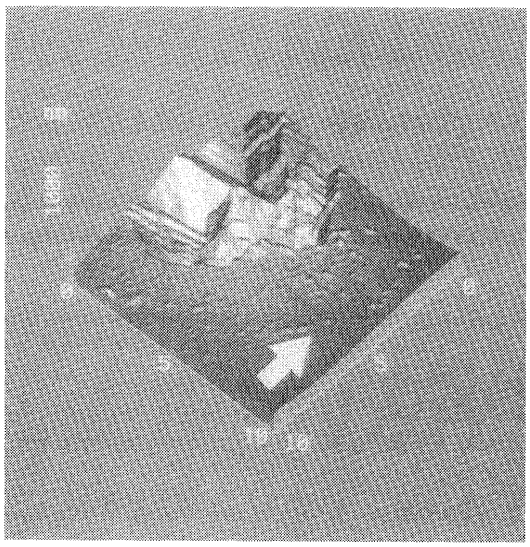

Fig. 8 Measured results of cyclic-bending

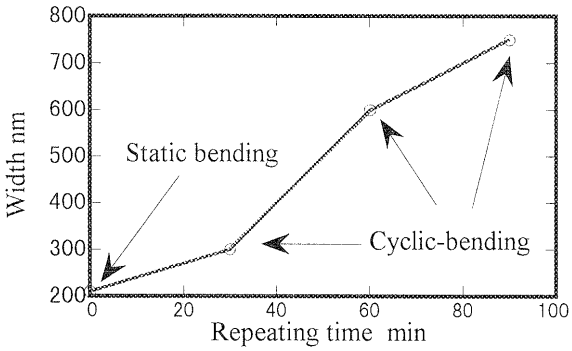

Fig. 9 Change in depth of defects versus repeating time

It has been reported that thermal vibration accelerates surface defects, especially plastic deformation[9]. In the present study, we investigated the influence of cyclic-bending on micro-defects. A sample, which had been indentated by a hardness tester (DUH-201)[10], was placed on the AFM bending unit. The variation of plastic defects (dislocation) around the corners of the indentation mark, which are illustrated in Fig. 10, was observed using AFM before and after bending, respectively. Figure 11(a) shows the result measured before bending, and Fig. 11(b) shows that measured after cyclic-bending for 90 minutes. It can be seen that plastic defects were

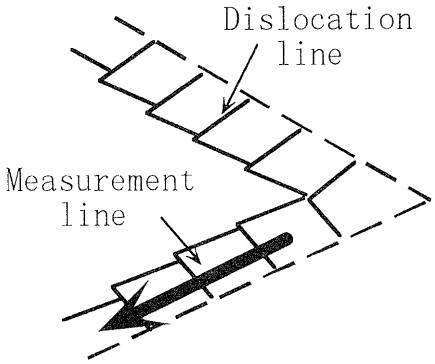

Fig. 10 The method of analysis obtained data

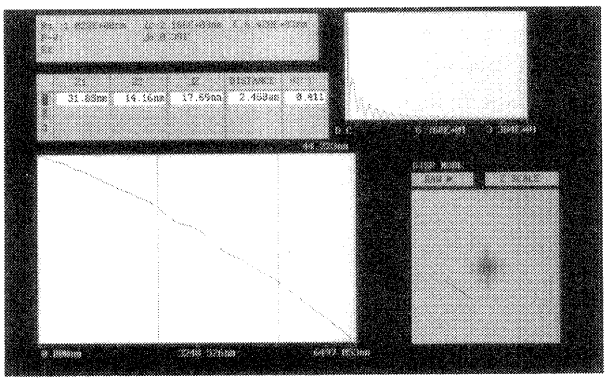

(a) before

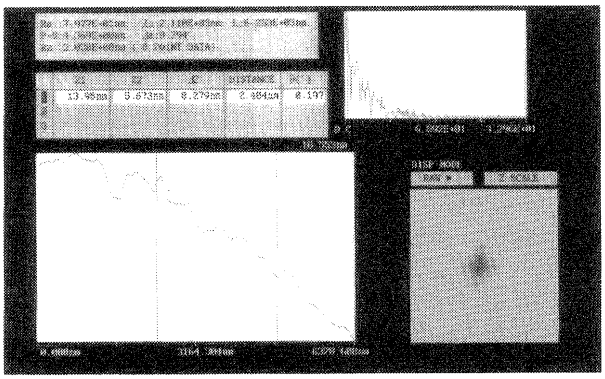

(b) after

Fig. 11 Results measured before and after cyclic-bending

enlarged by cyclic-bending.

4. Conclusions

The above results are summarized as follows:

(1) A new system that can measure micro-defects during the bending process has been designed and developed.

(2) Basic performance of the system has been investigated theoretically and experimentally.

(3) Potential micro-defects on a scratched surface and on an indentated surface were successfully observed.

References

(1) Takahasi, S., Miyoshi, T. and Takaya, Y., Study on Nano-Inprocess Measurement of Silicon Wafer Surface Defects by Laser Scattered Pattern, Proc, of ISMT'2, Japan, (1996), p. 243-250.

(2) Joe, A. and Ikeda, I., Aprecise Measurement of Deflection Occurred by Repeat Loading for Brittle Materials, J. Japan Soc. Prec. Eng., Vol. 59, No. 7 (1993), p. 1085-1090.

(3) Groot, P.D. and Deck, L., Surface Profiling by Analysis of White-Light Interferograms in the Spatial Frequency Domain, J. Modern Optics, Vol. 42, No. 2 (1995), p. 389-401.

(4) Page, T.F., The Deformation Behavior of Ceramic Crystals Subjected to Very Low (Nano) Indentation, J. Mater. Res., Vol. 7, No. 2 (1992), p. 450-471.

(5) Kalnas, C.E., Mansfield, J.F., Was, G.S. and Jones, J.W., In Situ Bend Fixture for Deformation and Fracture Studies in the Environmental Scanning Electron Microscope, J. Vac. Sci. Technol. A, Vol. 12, No. 3 (1994), p. 883-885.

(6) Rozlosnik, N., Bohus, L.S., Birattari, C. and Gadioli, E., Direct Observation of Latent Nuclear Tracks in Organic Material by Atomic Force Microscopy, Nanotechnology, Vol. 8 (1994), p. 32-34.

(7) Timoshenko, S.P. and Young, D.H., Element of Strength of Materials, Maruzen Asian Edition, p. 197.

(8) Kweon, H.K., Kuriyagawa, T. and Kiyono, S., Basic Study of Micromechanical Processing, Proc, of ICPE '96, China, p. 211-214.

(9) Matsuoka, S., On the Current State of Observation and Evaluation of Metal and Ceramics Samples by STM/AFM, Optical and Electro-Optical Engineering Contact, (in Japanese), Vol. 35, No. 5 (1996), p. 9-15.

(10) Catalog, Shimadzu Dynamic Ultra Micro Hardness Tester DHU Series, Testing machines plant Shimazu Corporation Kyoto Japan, 1995.